ADVANCED MATERIALS
www.advmat.de

Low Temperature Casting of Graphene with High Compressive Strength

Hengchang Bi, Kuibo Yin, Xiao Xie, Yilong Zhou, Neng Wan, Feng Xu, Florian Banhart, Litao Sun, and Rodney S. Ruoff**

Graphene, a 2-dimensional atom-thick layer of carbon atoms,[1–5] has attracted attention due to its fascinating properties such as high carrier mobility,[6–8] high thermal conductivity,[9,10] extraordinary elasticity and stiffness[11] and other properties. While mechanical exfoliation,[6] liquid exfoliation,[12] and epitaxial growth[13] can produce pristine graphene, graphene yields are currently too low for large-scale production of macrostructures. In contrast, chemical reduction of graphene oxide provides 'graphene' sheets in large scale for graphene macrostructures.[14–16] Graphene-based macrostructures prepared to date have been relatively weak mechanically, given their flexible and often relatively porous or open structures,[17–26] particularly with respect to compressive strength when compared with commercial graphite products.[27–29] Achieving highly compacted and thus "fully dense" macrostructures based on graphene and measuring the physical properties of such material(s) is thus an important goal.

Here, we report a pH-mediated hydrothermal reduction which is combined with moulding methods and allows controllable fabrication of compact high density graphene macrostructures with various shapes. The compact graphene (CG) product that is fabricated in this study shows great advantages over hitherto reported 3-D graphene products,[17–26] *e.g.*, a solid microstructure and a high density (~1.6 g cm^{-3}) which is comparable to conventional graphite products[27–29] and an ultrahigh compressive strength (~361 Mpa) which is 6 times higher than conventional graphite products and approx. 3 orders of magnitude higher than that of previously reported 3-D graphene.[21] Compared with conventional strategies for forming 3D shapes from graphite powder,[30–34] the method of this study allows to produce desired shapes via moulding in a single-step, low-cost, time- and energy-saving, and low-temperature process (180 °C). The CG macrostructures reported herein can thus be expected to promote new applications for graphene and further accelerate the commercialization of graphene-based products.

The synthesis of CG is described as follows: Graphite powder was oxidized through modified Hummers method into graphite oxide (GO). Then GO powder was dispersed in ultrapure water and sonicated and exfoliated, forming a brown colloidal aqueous dispersion of graphene oxide (G-O) platelets. Colloidal G-O suspension was transferred to a sealed reactor, ammonia or NaOH was added and the reactor heated sufficiently to remove the functional groups of G-O, reducing G-O into reduced graphene oxide (rG-O) platelets, which we hereafter refer to as 'graphene'. Graphene gel was then taken out of the reactor and dried at a temperature slightly higher than room temperature. Figure S1 illustrates the process of casting of such graphene platelets, where the dispersion of G-O platelets was placed into a screw-like, sealed container and was chemically reduced at 180 °C, after which it is black or dark grey. The resulting graphene gel was cast into a screw stem. For convenience, CG with the proper, excess, and no ammonia content were abbreviated as CGP (pH = 10.1), CGE (pH = 11.6), and CGN (pH = 5.5), respectively.

"Graphene castings" can be easily produced by this approach compared to other methods (see Experimental, and Figure S2 in Supporting Information). Different castings were made, e.g., triangular prism, quadrangular prism, joint ring, crucible, screw stem, and gear, as shown in **Figure 1**. The dimension of castings ranges from sub-millimeter to centimeter, which depends on the mould and the concentration of G-O. As long as the concentration of the G-O dispersions is above 0.5 mg mL^{-1},[19] the resulting graphene gel can be cast into any complicated macroscopic shape.

Based on a series of experiments for different reaction times, a process flow of the forming of the castings was optimized and is shown in Figure 1g. First, the aqueous dispersion of G-O platelets (G-O sol) was placed in a sealed reactor and then heated at 180 °C for 1 to 3 h; the dispersion became dark brown and more viscous initially, and then black. We suggest that the removal of oxygen-containing functional groups results in a degree of cross-linking between some of the platelets, thereby increasing the viscosity and under further removing of O-containing functional groups with still further cross-linking,

Prof. L. T. Sun, H. C. Bi,[+] Dr. K. B. Yin,,[+] Dr. X. Xie, Dr. F. Xu, Y. L. Zhou, Dr. N. Wan
SEU-FEI Nano-Pico Center
Key Laboratory of MEMS of Ministry of Education
Southeast University, Nanjing 210096, P. R. China
Tel: 86-025-83792632-8813,
Fax: 86-025-83792939
E-mail: slt@seu.edu.cn
Prof. R. S. Ruoff
Department of Mechanical Engineering and Materials and Science Program
The University of Texas at Austin
One University Station C2200
Austin, TX 78712, USA
E-mail: r.ruoff@mail.utexas.edu
Prof. F. Banhart
Institut de Physique et Chimie des Matériaux
UMR 7504 CNRS
Université de Strasbourg
23 rue du Loess, 67034 Strasbourg, France
[+] These authors contributed equally to this work.

DOI: 10.1002/adma.201201519

ADVANCED MATERIALS
www.advmat.de

www.MaterialsViews.com

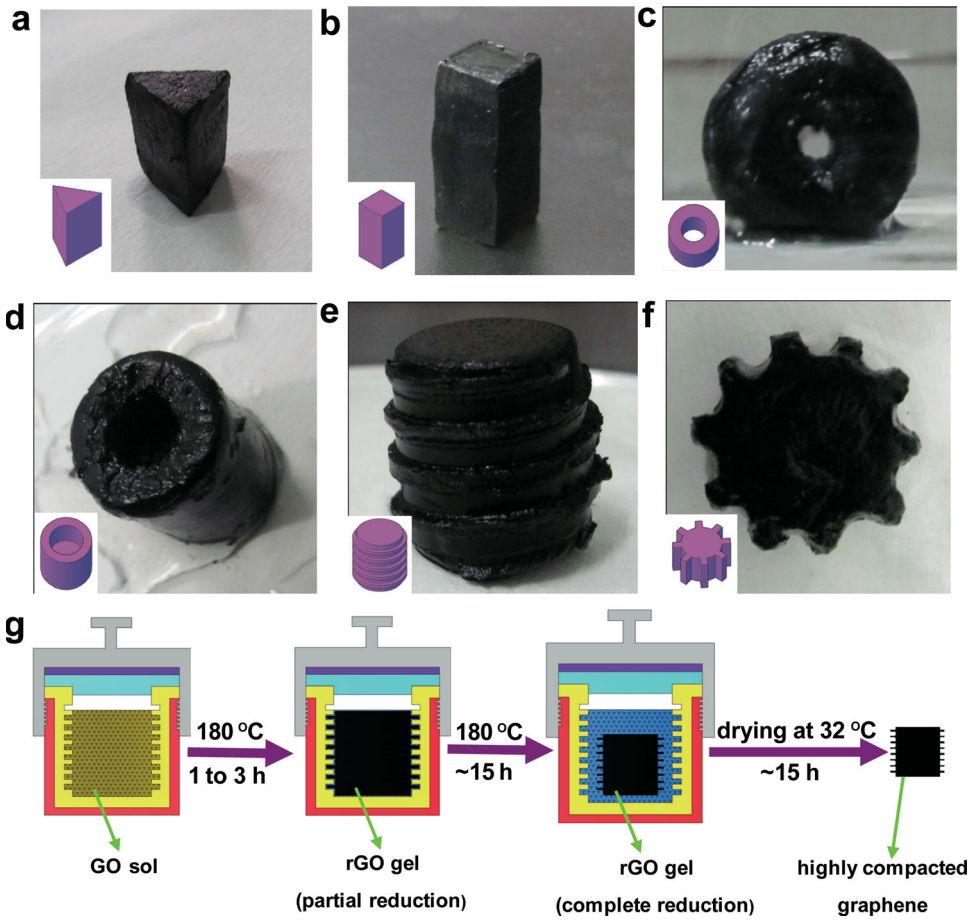

Figure 1. Different castings of the graphene before drying; (a) triangular prism, (b) quadrangular prism, (c) joint ring, (d) crucible, (e) screw stem, (f) gear. The insets at the bottom-left corner are their three dimensional concept maps, respectively. (g) Diagram of the procedure of castings which comprises four steps: 1) G-O dispersed in dH_2O; 2) rG-O gel with partial reduction indicated by local magnified image; 3) rG-O gel with complete reduction; 4) final casting with densified structure. The names of each part in Figure 1g are detailed in the Figure S1.

rendering the G-O platelets more hydrophobic (rG-O gel gradually formed). Graphene platelets evidently combine together, which squeezes water out and, it suggested, completes the reduction of the rG-O gel as well as further shrinkage. The linear dimension changed into 1/2-1/3 of the original G-O sol in this step. Finally, graphene gel was taken out from the sealed reactor and dried for 15 h at 32 °C in a drying oven with a stable air flow, resulting in further shrinkage of the dimensions to 1/4 compared to the wet gel. At the same time the density of the dried casting increased to 1.4–1.6 g cm^{-3}. It was found that the final shape of the casting matched the shape of the reaction vessel. After being reduced into graphene gel, the shape of the casting was fixed; further dehydration in the drying oven did not change its shape, but it further contracted and more water was driven out by heating. After drying the mechanical and electrical properties of the castings were then determined. CG obtained from G-O dispersions with pH 10 had a density of ranging from 1.4 g cm^{-3} to 1.6 g cm^{-3}, which is comparable to conventional graphite products (1.54-1.78 g cm^{-3})[27–29] and is denser than other isotropic 3D-graphene macrostructures.[21–23,25,26] CG also has a high compressive strength ranging from 318 to 401 MPa, with an average value of 361 MPa about ~6 times that of conventional graphite products,[27–29] and 2 to 8 times larger than isostatically pressed graphite (45–196 MPa).[35–39] High-resolution transmission electron microscopy (HRTEM) and scanning electron microscopy (SEM) helped to explain the high density and compressive strength (Figure S3, and Figure S4). The graphene platelets which have been used possess a typical size ranging from tens of nanometers to hundreds of nanometers (Figure S3). The graphene platelets seem to seamlessly bond to each other, with no void observed even at a magnification of 15,000X (Figure S4a), whereas typical 3D-graphene macrostructures made to date, and isotropic graphite parts, are microporous as shown in even low magnification (~50X).[21,23,25] However, with magnification 50,000X, compact and isotropic cross-linking of graphene sheets can be clearly seen (Figure S4a, Figure S4b), which explained the high density and high compressive strength of CG castings. Besides, the microstructure of CG was also investigated by XRD and Raman spectroscopy, as shown in Figure S5, and Figure S6, respectively. The basal spacing of CG was nearly comparable with that of graphite. The Raman spectrum of CG showed that the D band intensity was

DOI: 10.1002/adma.201201519

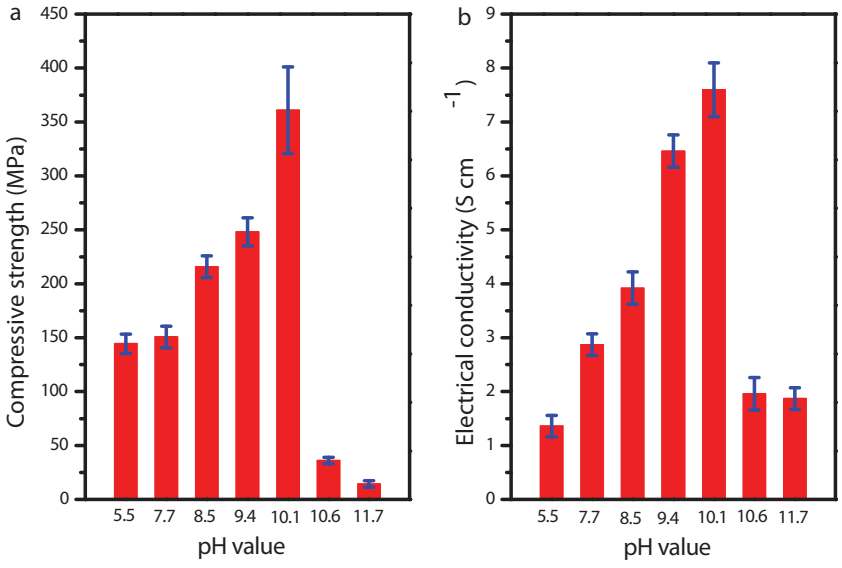

Figure 2. Impact of pH on compressive strength and electrical conductivity after annealing (900 °C): (a) Compressive strength versus pH. (b) Electrical conductivity versus pH. It is clearly seen that optimum pH = 10 for better compressive strength and electrical conductivity. Besides, annealing at high temperature was also proved helpful to compressive strength and electrical conductivity compared to Figure S7.

almost equal to the G band intensity, which indicated the small average size of the sp^2 domains (Figure S6).

CG has an electrical conductivity (7.1–8.2 S cm^{-1}) comparable to graphene foam prepared by chemical vapour deposition,[25] and 6 orders of magnitude higher than chemically derived graphene-based composites.[40] CG also has high thermostability per thermogravimetric (TG) and differential thermogravimetric (DTG) measurement obtained from CGN (pH ~5.5) and CGP (pH ~10) samples. (Figure S7). CG lost ~6 wt% in the range below 100 °C due to the removal of adsorbed water, while a steady mass loss was observed in the range of 300–700 °C, which was ascribed to the decomposition of the oxygen functional groups that had survived the hydrothermal reduction.[41,42] The heating rate was 10 °C min^{-1} and the TG curves showed CGP was more stable than CGN since CGP lost 17% mass at 700 °C while CGN lost 23%. In addition, CG after annealing (900 °C) was more stable.

During the repetitive synthesis of CG, the effect of pH on the physico-chemical quality of castings has emerged. Relationships between compressive strength, conductivity and pH have then been studied. In this section, CG was obtained from G-O dispersions with different pH values adjusted by ammonia (pH 5.5 ~ 10.1) or sodium hydroxide (pH 10.7 ~ 11.6). The compressive strength of CGN (pH = 5.5, 124.3MPa) was apparently smaller than that of CGP (pH = 10.1, 211.4 MPa), indicating the contribution of proper pH to improvement of compressive strength. According to the results, the CG would achieve maximum compressive strength when the pH of G-O dispersion was adjusted to 10 (Figure S8a). With the help of the annealing, the compressive strength can be further improved. For example, the compressive strength of aforementioned CGP reached to 361 MPa (maximum 401 MPa) (**Figure 2**a). Electrical conductivity of CG was found greatly affected by pH as well. The maximum conductivity for CG (pH = 10) is up to 1.12 S cm^{-1}, which was at least two times as great as that of CGN (Figure S8b). Similarly, high temperature annealing played a key role in improvement of the conductivity. The conductivity increased to 7.6 S cm^{-1} for CG (Figure 2b) after annealing, which is very close to that of graphene foam.[25]

In order to clarify the relationship between pH and mechanical property of CG, SEM was applied to study the surface morphology and structure of cross-section. Images of the surfaces of CG demonstrated the importance of pH. Rugged CGN surface accompanied with pits throughout the surface was observed (**Figure 3**a). There were also many but smaller protuberances on the surface of CGE (Figure 3b), which may imply the fact that a great deal of ammonia vapor had escaped from graphene gel during solidification. Contrarily, CGP appeared a smooth surface (Figure 3c). Similar phenomenon was also observed in the digital photographs (Figure S9). Figure 3d and 3e

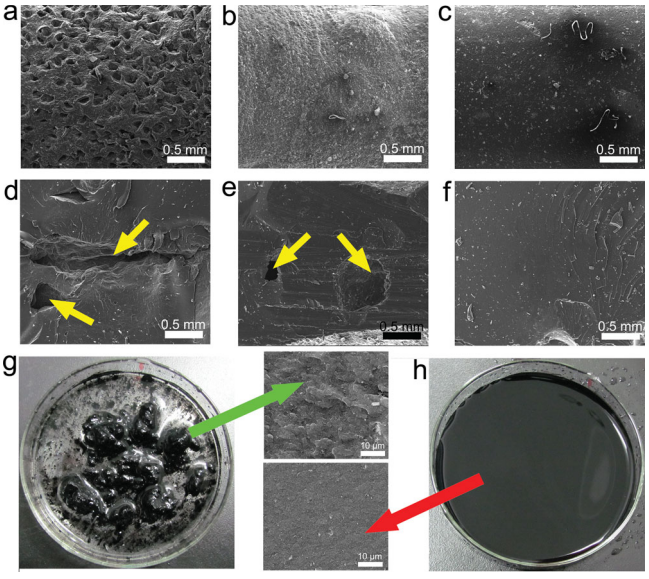

Figure 3. SEM images of surface and cross-section of CG. Photographs for the reaction stopped at 45 minutes. (a-c) surfaces. (a) CGN, rough surface on which holes could be observed. (b) CGE, rough surface on which protuberances could be observed. (c) CGP, smooth surface was produced when pH = 10. (d-f) cross-sections. (d) CGN, holes and cracks inside indicated by arrows. (e) CGE, imperfections were observed, indicated by arrows. (f) CGP, graphene sheets combined solidly. No imperfection was found in this case. (g) CGN, G-O sheets aggregated into domains forming bigger particles. Consequently, the cross-section of CGN indicated by green arrow mainly consisted of fish-scale carbon, presenting significant roughness. (h) CGP, G-O sheets homogeneously dispersed into the viscous solution due to the negative charges of all the sheets. With the proceeding of reaction, CGP was made up of individual graphene sheets. Based on this fact, the cross-section of CGP indicated by red arrow was smooth due to the homogeneous distribution of smaller carbon particles.

demonstrated that either shortage or excess of ammonia led to the formation of holes and cracks within the CG during agglomeration of graphene sheets. These imperfections could decrease density, compressive strength and conductivity. A dense structure of CGP without apparent imperfection can be acquired with a proper pH (Figure 3f). Comparisons among the cross-sections of the three CG further proved that the quantity of ammonia, in another word, the pH played a critical role during the agglomeration of graphene sheets, and had further impact on the performance of CG. Moreover, CGN and CGP obtained from the hydrothermal reaction for 45 minutes were investigated by naked eye (Figure 3g, and Figure 3h). At this time point, graphene sheets began to aggregate for CGN, but not for CGP. The graphene sheets in Figure 3h agglomerate together as a whole due to negative charges on every graphene sheets, which lead to a homogeneous dispersion. It has been reported that proper quantity of ammonia corresponding to pH = 10 yielded the maximal charge density on graphene sheets.[43] Cross-sections of CGN (indicated by green arrow) and CGP (indicated by red arrow) were also characterized by SEM with apparent differences corresponding to Figure 3g and Figure 3h, respectively. The cross-section of CGN consists mainly of fish-scale carbon with significant roughness, whereas CGP had a smoother cross-section due to the uniformity of smaller carbon particles. As a result, the mechanical and electrical properties of CGP are better than that of CGN. In addition, no mesh-like structures were observed for CGN and CGP.[21–23]

Due to their strong hydrophilicity and electrostatic repulsion effects, G-O sheets can easily be uniformly dispersed in water. However, different quantities of ammonia exert different electrostatic repulsion effects on the sheets.[43] Similar effects (various pH) on the multi-wall carbon nanotube (MWCNT) can be found elsewhere.[44] Carboxylic acid groups attached to G-O sheets could ionize, resulting in carboxylic ions containing negative charges. This detail is described in equation (1). In pure water, few carboxylic acid groups ionize. That is, minor G-O sheets have negative charges, while most of the sheets do not. When ammonia was added to the solution, another reaction occurs, as shown in equation (2).

$$\text{R-COOH} \rightleftharpoons \text{R-COO}^- + \text{H}^+ \quad (1)$$

$$\text{NH}_3 \cdot \text{H}_2\text{O} \rightleftharpoons \text{NH}_4^+ + \text{OH}^- \quad (2)$$

The combination of H^+ and OH^-, which results in water, promotes the forward reaction of the two equations. Therefore, the majority of the sheets would possess negative charges.

Meanwhile, the degree of ionization decreases with increasing quantity of ammonia. Figure S10 shows schematic changes in the ionization of COOH with increasing quantity of ammonia. In the same figure, other oxygen functional groups are hidden intentionally. When the pH is adjusted to be around 10, the ionization degree is at a maximum (Figure S10b).[43] For pure water (the pathway indicated by black arrows in **Figure 4**), before reduction, G-O sheets are dispersed well due to hydrophilic functional groups. As the reaction progresses, for example, reaction for tens of minutes, some carboxylic groups are removed, which decreases the charges of some G-O sheets. In addition, G-O sheets without any charge tend to be attracted to those with charges to form large sheets. Large sheets that possess charges still disperse into the water due to electrostatic repulsion effects. According to the XRD patterns (Figure S5) and IR spectra (Figure S11) obtained from the CG, many hydrophilic functional groups are eliminated by a long reaction time (15 h). This elimination brings about two results: the hydrophobic nature of G-O sheets is enhanced, and the electrostatic repulsion effects become weak due to the removal of carboxyl groups. Both of the results are beneficial for the agglomeration of graphene sheets. Because the sample consists of large graphene sheets, the surface becomes rough and exists many holes inside (see Figure 3). Meanwhile, the conductivity and strength of the sample tend to be poor, which is attributed to the wide space between graphene sheets. When electrons pass through the sheets, the space increases the scatter probability and hinders the motion of the electrons. When the pH is adjusted to around 10 by the addition of ammonia (the pathway indicated by green arrows in Figure 4), the sheets do not agglomerate partially but come together simultaneously as a whole with the progress of reaction and evaporation of water. When most of the carboxylic acid groups are removed, Van der Waals forces would exceed the electrostatic repulsion forces. All the graphene sheets agglomerate together in a compact manner. Thus, the space between sheets is minimized during agglomeration, which contributes to the enhancement of conductivity, density, and strength. Excess ammonia leads to a decrease in ionization degree, resulting in the tendency of the surface of sample to become rough and deterioration of the electrical conductivity and compressive strength.

In summary, a feasible method for CG fabrication has been developed, whose production showed that the pH of the graphene oxide dispersions a key factor which determined properties of its product. pH has a direct impact on surface topography, internal structure, thus electrical and mechanical properties of the CG. CG has the most solid structure and properties when the pH of reaction was adjusted to 10, i.e., smooth surfaces, dense internal structures, good electrical conductivity, and high compressive strength. Even the density, compressive strength, and electrical conductivity have been further improved (1.6 g cm^{-3}, 361 MPa, and 7.6 S cm^{-1}, respectively) by high temperature annealing at 900 °C. In addition, it is found that CGP has a very high C atom concentration (Figure S12), which is beneficial for its mechanical and electrical properties. Meanwhile, the proposed method tended to be low-cost, environment-friendly, and energy-saving. CG is expected a great potential to be applied into a wide range of fields from traditional graphite industry (highly stable graphite heaters, electrodes, crystallizers, and anti-wear mechanical parts, *etc.*) to aerospace, atomic energy and nuclear science. This work also pointed a new route to prepare highly compressed and super strong three-dimensional carbon macrostructures based on graphene.

Adv. Mater. **2012**,
DOI: 10.1002/adma.201201519

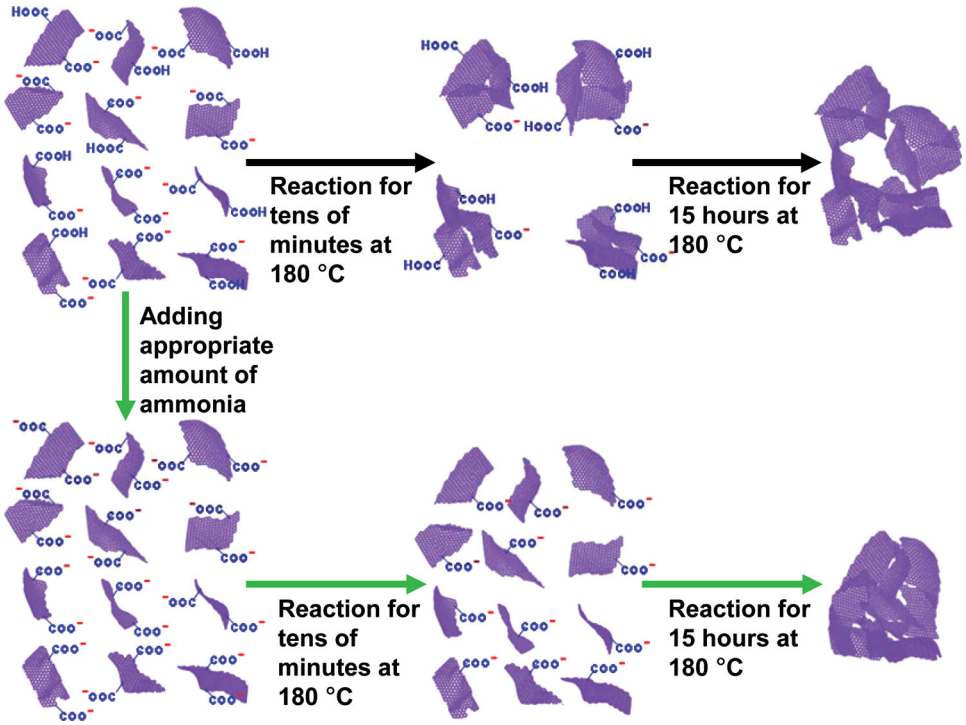

Figure 4. Process of agglomeration with the addition of different quantities of ammonia. Process of agglomeration of CGN was demonstrated by the path of black arrows. Most G-O sheets without charge were first attracted to minor G-O sheets with negative charges and became large sheets. Due to the removal of carboxyl groups, the large G-O sheets finally lost charges and agglomerated easily. Process of agglomeration of CGP was indicated by the path of green arrows. The carboxyl groups ionize into COO^-, which reduced the partial agglomeration of the initial minor G-O sheets. The G-O sheets became hydrophobic and COO^- groups were removed gradually, resulting in a uniform agglomeration of G-O sheets in a compact manner.

Experimental Section

Preparation of Graphite Oxide (GO): GO was prepared by oxidizing graphite (EG) powder based on Hummers method.[45] The detail can be described as follows. Expandable graphite powder (2 g) and sodium nitrate (1 g) were mixed, sulfuric acid (46 mL, 98 wt%) was added in an ice bath. Potassium permanganate (6 g) was slowly added to the mixture to prevent the temperature from exceeding 20 °C. After reaction at 35 ± 1 °C for 8 h with gas release, deionized water (dH_2O, 92 mL) was gradually added, bringing about violent effervescence. The temperature of the waterbath was then increased to 95 °C for 15 min in order to increase the degree of oxidation of the GO product. Bright-yellow suspension was diluted with dH_2O (280 mL) and was further treated with H_2O_2 (30%, 6 mL). GO sheets were collected by filtration and washed 7 times with hydrochloric acid (5 v/v%) until no sulphate could precipitate in the presence of $BaCl_2$. GO was washed 7 times with dH_2O to remove chloride ions and dried overnight in an oven at 60 °C.

Fabrication of CG: Colloidal dispersion of G-O was hydrothermally reduced in dH_2O with different amounts of ammonia. In each case, 57 mg of GO was dispersed in 35 ml dH_2O with ammonia (25-28 v/v%) followed by sonication for 15 min. Dark brown colloidal dispersion was transferred to a sealed reactor which was then heated to 180 °C for 15 h. After heat treatment, the reactor was left to room temperature. In order to fabricate castings, plastic containers with complex shapes were designed (Figure S2). The reduced graphene suspension was moulded in the container and was treated in an air drier at 32 °C for at least 15 h for completely drying the casting.

Characterization of CG: The XRD patterns of the CG (5 °–60 °) were measured using an Arl X'TRA diffractometer with an output power of 2.2 kW. CG was filtrated and purified many times and then were ground to powder using pestle and mortar. The IR spectroscopy (400–4000 cm^{-1}) was performed using a Nicolet IR 870 FI-IR spectrometer with pure KBr as the background. Repetitive filtrations were carried out before being ground with KBr for sample preparation. Then the grounded powder was dried and shaped into a transparent tablet for measurement. Morphology of CG was characterized using a Quanta 200 scanning electron microscope (SEM) under an accelerating voltage of 20 kV. The SEM specimens were prepared by drying the CG directly and then breaking them into two halves for investigation of cross-section. To study the structure of graphene castings, the powder of castings were collected on a copper grid for TEM analysis using Titan 80-300 with spherical abbreation (Cs) corrector.

Measurements of Apparent Density, Mechanical, Electrical Properties and Thermostability: In order to measure the density of CG, the samples were fabricated into regular cylinders, whose weight and dimensions (height, and diameter) were acquired by using an electronic scale and a vernier caliper, respectively. Several samples under the same reaction condition were measured. Compressive mechanical measurements were performed using an electronic universal testing machine (CMT 4503, Shenzhen Xinsansi, China) with two test plates. The graphene sheets were fabricated into solid cylinders (height of 4 mm; diameter of 4 mm), with the condition that the two end faces of the solid cylinders must be parallel to each other. A solid cylinder was set on the lower plate of the machine and compressed by the upper plate, which was connected to a load cell, until it was crushed. The dropping velocity of the upper plate was set to be 1 mm min^{-1} during the measurements. Electrical conductivity of CGN and CGP was measured by a two-probe method. During measurement, copper wires were embedded and connected to the CG with silver paste, enabling stable electrical contact between copper wires and CG. Resistance was read out directly and was converted into conductivity. Thermogravimetric analysis was performed with a

PerkinElmer TGA Pyris1 instrument filled with nitrogen and heating rate was set at 10 °C min^{-1}.

Supporting Information

Supporting Information is available from the Wiley Online Library or from the author.

Acknowledgements

This work was supported by the National Basic Research Program of China (Grant Nos. 2011CB707601 and 2009CB623702), the National Natural Science Foundation of China (Nos. 51071044, 60976003, 61006011 and 61106055), Specialized Research Fund for the Doctoral Program of Higher Education (Nos. 20100092120021 and 20100092110014) Program for New Century Excellent Talents in University (No. NCEF-09-0293) and Open Research Fund of State Key Laboratory of Bioelectronics.

Received: April 16, 2012
Published online:

[1] Y. W. Zhu, S. Murali, W. W. Cai, X. S. Li, J. W. Suk, J. R. Potts, R. S. Ruoff, *Adv. Mater.* **2010**, *22*, 3906.
[2] D. R. Dreyer, R. S. Rouff, C. W. Bielawski, *Angew. Chem. Int. Ed.* **2010**, *49*, 9336.
[3] A. K. Geim, K. S. Novoselov, *Nat. Mater.* **2007**, *6*, 183.
[4] A. K. Geim, *Science* **2009**, *324*, 1530.
[5] A. Savchenko, *Science* **2009**, *323*, 589.
[6] K. S. Novoselov, A. K. Geim, S. V. Morozov, D. Jiang, Y. Zhang, S. V. Dubonos, I. V. Grigorieva, A. A. Firsov, *Science* **2004**, *306*, 666.
[7] K. S. Novoselov, A. K. Geim, S. V. Morozov, D. Jiang, M. I. Katsnelson, I. V. Grigorieva, S. V. Dubonos, A. A. Firsov, *Nature* **2005**, *438*, 197.
[8] Y. Zhang, Y. W. Tan, H. L. Stormer, P. Kim, *Nature* **2005**, *438*, 201.
[9] A. A. Balandin, S. Ghosh, W. Z. Bao, I. Calizo, D. Teweldebrhan, F. Miao, C. N. Lau, *Nano Lett.* **2008**, *8*, 902.
[10] R. Prasher, *Science* **2010**, *328*, 185.
[11] C. Lee, X. D. Wei, J. W. Kysar, J. Hone, *Science* **2008**, *321*, 385.
[12] Y. Hernandez, V. Nicolosi, M. Lotya, F. M. Blighe, Z. Y. Sun, S. De, I. T. McGovern, B. Holland, M. Byrne, Y. K. Gun'ko, J. J. Boland, P. Niraj, G. Duesberg, S.Krishnamurthy, R. Goodhue, J. Hutchison, V. Scardaci, A. C. Ferrari, J. N. Coleman, *Nat. Nanotechnol.* **2008**, *3*, 563.
[13] P. W. Sutter, J. I. Flege, E. A. Sutter, *Nat. Mater.* **2008**, *7*, 406.
[14] W. Gao, L. B. Alemany, L. J. Ci, P. M. Ajayan, *Nat. Chem.* **2009**, *1*, 403.
[15] V. H. Pham, T. V. Cuong, T. Nguyen-Phan, H. D. Pham, E. J. Kim, S. H. Hur, E. W. Shin, S. Kim, J. S. Chung, *Chem. Commun.* **2010**, *46*, 4375.
[16] H. L. Wang, J. H. Robinson, X. l. Li, H. J. Dai, *J. Am. Chem. Soc.* **2009**, *131*, 9910.
[17] D. A. Dikin, S. Stankovich, E. J. Zimney, R. D. Piner, G. H. B. Dommett, G. Evmenenko, S. T. Nguyen, R. S. Ruoff, *Nature* **2007**, *448*, 457.
[18] S. J. Park, N. Mohanty, J. W. Suk, A. Nagaraja, J. An, R. D. Piner, W. W. Cai, D. R. Dreyer, V. Berry, R. S. Ruoff, *Adv. Mater.* **2010**, *22*, 1736.
[19] A. R. Ranjbartoreh, B. Wang, X. P. Shen, G. X. Wang, *J. Appl. Phys.* **2011**, *109*, 014306.
[20] H. Q. Chen, M. B. Miiller, K. J. Gilmore, G. G. Wallace, D. Li, *Adv. Mater.* **2008**, *20*, 3557.
[21] Y. X. Xu, K. X. Sheng, C. Li, G. Q. Shi, *ACS Nano* **2010**, *4*, 4324.
[22] X. T. Zhang, Z. Y. Sui, B. Xu, S. F. Yue, Y. J. Luo, W. C. Zhan, B. Liu, *J. Mater. Chem.* **2011**, *21*, 6494.
[23] Y. X. Xu, Q.Wu, Y. Q. Sun, H. Bai, G. Q. Shi, *ACS Nano* **2010**, *4*, 7358.
[24] O. C. Compton, S. T. Nguyen, *Small* **2010**, *6*, 711.
[25] Z. P. Chen, W. C. Ren, L. B. Gao, B. L. Liu, S. F. Pei, H. M. Cheng, *Nat. Mater.* **2011**, *10*, 424.
[26] W. Lv, Y. Tao, W. Ni, Z. Zhou, F. Y. Su, X. C. Chen, F. M. Jin, Q. H. Yang, *J. Mater. Chem.* **2011**, *21*, 12352.
[27] http://www.geselectrodes.com/products/specialty-graphite/ (accessed June 2012).
[28] http://www.alibaba.com/trade/search/3ilp5tyfchms/graphite.html (accessed June 2012).
[29] http://www.graphitesales.com/data_sheets/gs_30.pdf (accessed June 2012).
[30] S. Maebara, M. Goniche, F. Kazarian, M. Seki, Y. Ikeda, T. Imai, B. Beaumont, *Rev. Sci. Instr.* **2005**, *76*, 053501.
[31] M. H. Bocanegra-bernal, *J. Mater. Sci.* **2004**, *39*, 6399.
[32] http://www.patentstorm.us/patents/5336520/fulltext.html (accessed June 2012).
[33] G. R. Peterson, *United States patent.* **1970**, 3517092.
[34] S. C. Lee, K. L. Kim, *Mater. Sci. Eng., A* **2008**, *498*, 359.
[35] http://www.bjgreatwall.cn/p11.aspx (accessed June 2012).
[36] http://www.tokaicarbon.com/fine_carbon_products.html (accessed June 2012)
[37] http://www.chinahorton.com/(accessed June 2012).
[38] http://www.poco.com/(accessed June 2012).
[39] http://www.mvivek.com/images/property_data.pdf (accessed June 2012).
[40] S. Stankovich, D. A. Dikin, G. H. B. Domment, K. M. Kohihaas, E. J. Zimney, E. A. Stach, R. D. Piner, S. T. Nguyen, R. S. Ruoff, *Nature* **2006**, *442*, 282.
[41] V. H. Pham, T. V. Cuong, T. Nguyen-Phan, H. D. Pham, E. J. Kim, S. H. Hur, E. W. Shin, S. Kim, J. S. Chung, *Chem. Commun.* **2010**, *46*, 4375.
[42] J. F. Shen, Y. Z. Hu, M. Shi, N. Li, H. W. Ma, M. X. Ye, *J. Phys.Chem. C* **2010**, *114*, 1498.
[43] D. Li, M. B. Muller, S. Gilje, R. B. Kaner, G. G. Wallace, *Nat. Nanotechnol.* **2008**, *3*, 101.
[44] N. B. Saleh, L. D. Pfefferle, L. D. Elimelech, *Environ. Sci. Technol.* **2008**, *42*, 7963.
[45] W. S. Hummers, R. E. Offeman, *J. Am. Chem. Soc.* **1958**, *80*, 1339.